

Large-scale magnetic fields and anomalies of chemical composition of stellar coronae

V.V. Pipin and V.M. Tomozov

Institute Solar-Terrestrial Physics, Irkutsk

Abstract

We present evidences that anomalies in abundance of the chemical minor elements with the low first ionization potential (FIP) in the low corona of the late-type stars can be related with topology of the large-scale magnetic field. The solar observations show the increased abundances of the low FIP elements in compare to the abundances of the high FIP elements above the active regions and in the closed magnetic configurations of the low corona. Observational data of Ulysses and the Stanford Solar Observatory show high correlations between FIP effect of the solar wind, amount of the unsigned open magnetic flux, and the ratio between strength of the large-scale toroidal and poloidal magnetic field on the surface. The solar-type stars show the increase abundance of the low FIP elements relative to elements with the high FIP with the decrease of the large-scale poloidal magnetic field (and increase the toroidal component of the magnetic field). The branch of the fully convective stars demonstrates inversion of the FIP-effect. This inversion can be result from strong coronal activity, which is followed to the strong poloidal magnetic on these stars.

Keywords: Sun-corona; solar-stellar analogy; magnetic fields; FIP effect

1. Introduction

Observations show that the stellar magnetic activity depends largely on the stellar mass and the rotational period (see, Donati and Landstreet, 2009; Vidotto et al., 2014; See et al., 2016). These parameters determine a power of dynamo processes (Noyes et al., 1984) and the typical topology of the large-scale magnetic field (Donati et al. 2008a; See et al. 2016). Therefore, we can, generally, expect that the chromospheric and coronal activity in late-type stars varies with the spectral class and rotational period, correspondingly (Reiners, 2012).

It is commonly known that chemical composition in the solar photosphere is spatially uniform. On other hand, Pottasch (1963) showed that the coronal chemical composition can depend on the first ionization potential (hereafter FIP). Moreover, elements with low FIP (≤ 10 eV), for example, Fe, Mg, Si, K etc, show increase of abundances in the coronal loops above the active regions.

At the same time, elements with high FIP ($\text{FIP} > 10 \text{ eV}$) show no variation or, sometimes, even a little decreased composition there. This is so-called 'FIP-effect' (Laming 2015).

Observations showed that elements with low FIP can be accumulated at top of the closed magnetic loops in course of the active regions evolution. For example, Widing and Feldman (2001) found that chemical composition of the coronal plasma above recently emerging active region is close to composition at the photosphere, and after that it shows increase concentrations of the elements with low FIP at the top of coronal loop. The ratio between the coronal and photospheric abundances of low FIP elements can reach factor 4 after a few days of evolution. Also, they found that in the long lived active regions the increase concentration of the elements with low FIP can reach factor 8 or even higher than that value.

The solar coronal regions with open magnetic fields (coronal holes) show almost no FIP effect. Fletcher et al. (2015) pointed out that chemical composition of plasma of the slow component of the solar wind shows an increase concentration of elements with low FIP by factor 3 compare to their values for the fast component of the solar wind. Contributions of the slow and fast components of the solar wind are closely related with budget of the closed and open magnetic flux of the Sun (Schatten et al. 1969). Thus, we can expect that the average FIP effect of the Sun as a star reflects the ratio between the closed and the open solar coronal magnetic field.

Wood et al. (2012) found a systematic decrease of the FIP effect with the stellar mass. Moreover, their results show inversion of the FIP-effect for the low mass M-dwarfs (inversed FIP effect). Origin of dependence of the coronal FIP effect with the spectral class of star is not clear. Results of Wood et al. (2012) were confirmed by Brooks et al. (2017), who also suggested existence of the solar cycle variations of the coronal FIP effect. The global parameters of the stellar magnetic activity changes with the stellar mass (Donati & Landstreet 2009). From earlier studies (see, e.g., Skumanich 1972; Noyes et al. 1984) we know that another critical parameter for stellar magnetic activity is the stellar rotation rate. Therefore observations of stellar coronal FIP elements anomalies and properties of the solar corona FIP fractionation suggested an interesting opportunity to study the stellar coronal FIP elements anomalies as a probe for topology of the stellar coronal field.

In this paper we analyse this idea using a combination of data from the study of Wood et al. (2012) and other data sets including the solar wind composition from the Ulysses space mission, the magnetic field observations from the Wilcox Solar Observatory, the stellar magnetic field spectropolarimetric measurements (see, Petit et al., 2014 and Marsden et al., 2014). In next section we will describe a database, which will be used in this study.

2. Data

The Table 1 gives list of the stars included in our analysis. The set covers range of spectral classes from the mid G to the mid M dwarfs. The color index

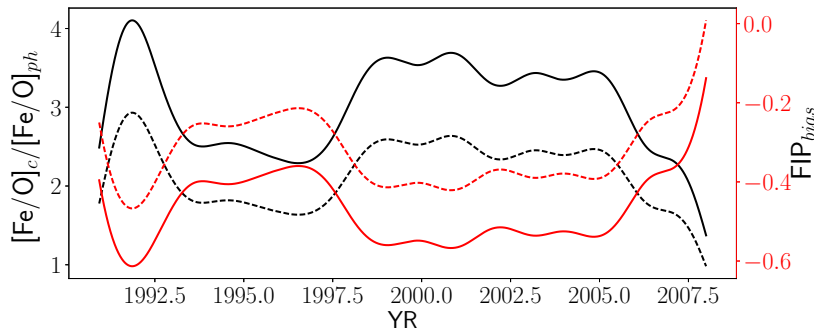


Figure 1: The FIP fractionation from Ulysses/SWICS after the Gaussian filtering (the dashed curve). The solid curve is obtained by cross-calibration with results of Laming (2015) and Brooks et al. (2017). The red line curves show the FIP_{bias} with magnitude shown by the right y-axis.

parameter B-V is taken from survey of Marsden et al. (2014). The data for FIP fractionation in stellar coronas are taken from Laming (2015). He used the results of several precedes see (Wood and Linsky, 2010; Wood et al., 2012). An interesting analysis of the FIP fractionation in solar and stellar magnetic activity was suggested recently by Brooks et al. (2017). Our data set includes less number of stars than theirs because magnetic parameters of stellar activity are not available for some of stars given in their papers. The next subsection describes how we the Ulysses/SWICS data set as well as solar magnetic field observations from was calibrated to the the Wilcox Solar Observatory.

2.1. Solar observations

To trace solar cycle variations of the FIP effect of the Sun as a star we use observations of Ulysses spacecraft. The data from instrument Ulysses/SWICS (Solar Wind Ion Composition Spectrometer) are used. It is assumed that in-situ measurements of the wind’s composition of heavy ions, e.g., such as O, C, and Fe, can be used to infer its composition in the low corona (Buergi and Geiss, 1986). In this paper we will use SWICS’s measurements for ions of Fe and O. The measurements procedure and their implications were described in details by Geiss et al. (1995) and von Steiger et al. (1995). The observed ratio (Fe/O) gives a proxy for the magnitude of the FIP fractionation in the solar corona. Following to procedure given by Wood et al. (2012) and Laming (2015) we introduce the so-called “FIP bias”. It is determined by ratio of the photospheric value of Fe/O and its coronal counterpart, i.e.,

$$FIP_{bias} = \log [Fe/O]_{ph} - \log [Fe/O]_c. \quad (1)$$

Here we assume that $\log [Fe/O]_{ph} = 0.06$ (Laming, 2015). The relative error of the SWICS’s measurements of the elemental composition is estimated to be 10-25% (see, e.g., Geiss et al., 1995).

Superposed epoch analysis of Geiss et al., 1995 showed rather tight correlation between magnitude of FIP fractionation and coronal structures related with regions of the fast and slow solar wind. Their results clearly showed that FIP fractionation is small in coronal holes. These solar phenomena are usually related with the open magnetic field structures. On other hand the FIP fractionation grows by factor 3-4 above the active regions, where the closed magnetic field structures dominate. This conclusion was further stressed by Fletcher et al. (2015).

The trajectory of Ulysses spacecraft passed over very different parts of the solar disk. To deduce the FIP effect for the Sun as a star we smoothed the data by the Gaussian filter with the FWHM equal one year. The result is shown in Figure 1 by the dashed lines. The graph shows that in the smoothed data the FIP fractionation had maximum magnitude of factor 3. It occurs near the maximum of the 23-d solar cycle. The corresponded value of FIP bias was about -0.4. Laming (2015) and Brooks et al. (2017) argued that the maximum FIP bias for the Sun as a star during epoch of solar maxims should be around -0.6 , i.e., the FIP fractionation should be factor 4. The reduced value in our case is explained by the strong smoothing applied to the original data. In our paper we consider the *relative* variations of the FIP effect in the solar cycle. By this reason, we deliberately multiply the observed ratio $[Fe/O]_{cr}$ by factor 1.4. This brings our data in agreement with estimations of Laming (2015) and Brooks et al. (2017). With this calibration we get FIP bias equals to -0.35 during the 23-d solar cycle minimum and -0.33 ± 0.05 during the exceptionally long minimum of the 24-th solar cycle. These estimations agrees with Brooks et al. (2017), as well.

Parameters of the solar magnetic field were determined using observations of the Wilcox Solar Observatory (WSO), see Duvall et al. (1979) and Hoeksema (1995). These data span about four solar cycles starting from 1976. The large-scale magnetic field was restored using the spherical harmonic coefficients obtained from the potential field extrapolation employing the so-called “source surface”. More details about procedure to determine the spherical harmonic coefficients decomposition can be found at the WSO web-site. Using the obtained distributions of the large-scale magnetic field we determine the unsigned open, $\Phi_o(t)$, the closed, $\Phi_c(t)$, and the total, $\Phi_s(t)$, magnetic fluxes as follows

$$\Phi_o(t) = R_s^2 \int |B_r(\theta, \phi, t)|_{r=R_s} \sin \theta d\phi d\theta, \quad (2)$$

$$\Phi_s(t) = R^2 \int |B_r(\theta, \phi, t)|_{r=R} \sin \theta d\phi d\theta, \quad (3)$$

$$\Phi_c(t) = \Phi_s(t) - \Phi_o(t) \quad (4)$$

where ϕ is longitude, θ is the polar angle and the source surface radius is $R_s = 2.5R$. Also we need a proxy for the ratio $\Phi_o(t)/(\Phi_s(t))$. For this we suggest to employ the mean magnitudes of the *axisymmetric* poloidal and total (axisymmetric and nonaxisymmetric) toroidal magnetic field, which are as follows, $\overline{B^{(PA)}} = \left\langle \sqrt{B_r^2(\theta, t) + B_\theta^2(\theta, t)} \right\rangle_{r=R}$, and $\overline{B^{(T)}} = \overline{|B_\phi(\theta, \phi, t)|}_{r=R}$, where,

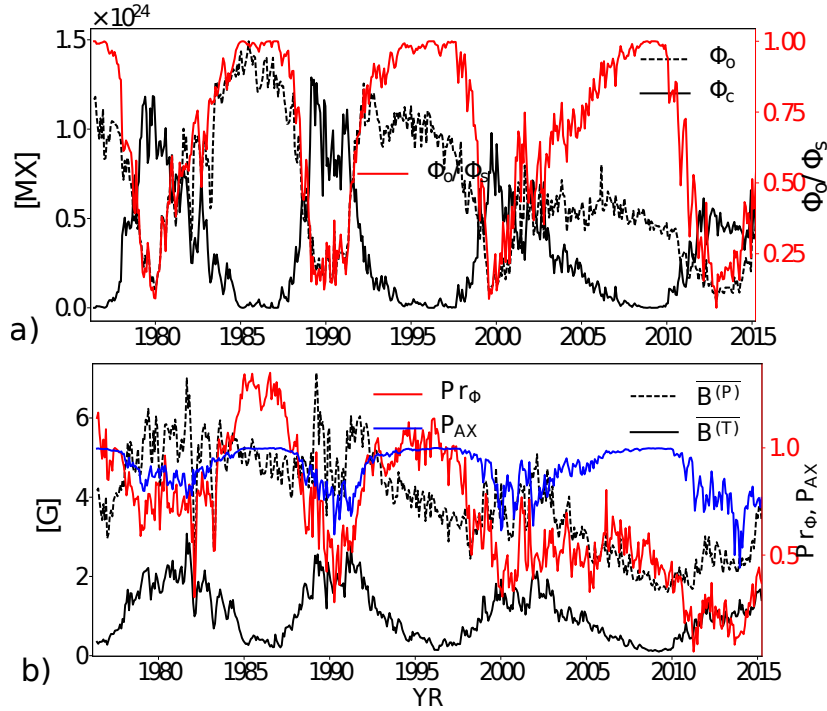


Figure 2: a) The unsigned open and closed magnetic fluxes and ratio $\Phi_o(t)/(\Phi_s(t))$ (red line, right scale) deduced from the WSO's harmonic coefficients; b) the mean components of the large-scale magnetic fields, index of the axisymmetric poloidal field, P_{AX} and the proxy Pr_ϕ (see, Eq6) shown by the red line.

$B_{r,\phi}$ are inferred from the same spherical harmonic coefficients. We introduce two parameters showing relative contribution of the axisymmetric poloidal field:

$$P_{AX} = \frac{\overline{B^{(PA)}}}{\overline{B^{(PA)}} + \overline{B^{(T)}}}, \quad (5)$$

and another proxy is defined as follows

$$Pr_\phi = P_{AX} \log \frac{(\overline{B^{(PA)}} + \overline{B^{(T)}})^2}{[G]^2}. \quad (6)$$

The reason to express the relative contribution of the axisymmetric poloidal magnetic field in form of Eq(5) is because it correlates well with Φ_o/Φ_s . The additional factor in Eq(6) reflects long-term changes of the magnetic activity. Figure 2 shows results for the defined parameters of the solar magnetic field. The budget of the unsigned magnetic flux through the solar surface is in a good agreement with Schrijver and Harvey (1994). The data presented in Figure 2 were further smoothed with the same Gaussian filter as the data about chemical composition.

	B-V	$\log \frac{\overline{B}^2}{[G]^2}$	$\overline{B^{(T)}}, [G]$	$\overline{B^{(P)}}, [G]$	$\overline{B^{(PA)}}, [G]$	FIP bias	P_{cyc}	Ref
χ^1 Ori	0.59	2.35	10	8.6	6.6	-0.555	16.8,L	[1,2]
		2.22	11	5.4	4.4			
		2.60	17	7.8	6.8			
		2.41	13	7.2	6.1			
EK Dra	0.61	3.63	61	19.2	17.8	-0.277	9.2,L	-/-
		3.90	74	36.6	34.3			
π^1 Uma	0.62	2.76	21	9.8	8.9	-0.645	2.1,L	-/-
Sun	0.66	1.16	0.94	3.4	2.77	-0.48	11	this work, [1,4]
κ^1 Ceti	0.68	2.88	21.7	16.9	9.5	-0.462	5.9,L	[1,2,3]
		2.64	17	8.6	7.7			
ξ Boo A	0.72	3.67	61.5	29.8	9.42	-0.32	4-5, 11,L	[1, 3]
AB Dor	0.86	4.92	152.6	244.7	73.1	0.488	18,L	[1,3]
		4.72	99.8	206.2	54.5			
ϵ Eri	0.88	2.27	3.86	13.1	4.1	-0.06	3,13,L	[1,3]
		2.08	3.3	13.2	10.1			
		2.50	13.6	11.4	9.7			
		2.09	5.6	9.5	7.6			
		2.63	13.8	15.3	10			
		2.66	10	18.9	8.6			
ξ Boo B	1.16	2.60	11.3	16.5	8.1	-0.18	4.3,L	[1,3]
EV Lac	1.36	5.54	131	573	306	0.474		[1,3]
AD Leo	1.54	4.76	33.6	237	230	0.536		[1,3]
EQ Peg A	1.58	5.31	156	423	357	0.450		[1,3]
EQ Peg B	1.7	5.35	67	468	451	0.417		[1,3]

Table 1: \overline{B} is the mean density of the large-scale magnetic field; $\overline{B^{(P)}}$ is the mean density of the large-scale poloidal magnetic field; $\overline{B^{(T)}}$ is the same for the axisymmetric poloidal magnetic field. List of our references for magnetic data and FIP bias is as follows: [1]Laming (2015); [2]Rosén et al. (2016); [3]See et al. (2015); [4]Brooks et al. (2017)

	Magnetic observations	Source	FIP _{bias}	Source
χ^1 Ori	2007.1, 2008.1, 2010.8, 2011.9	Rosén et al. (2016)	2001	Telleschi et al. (2005)
EK Dra	2007.1, 2012.1	-/-	2001	-/-
π^1 Uma	2007.1	-/-	2001	-/-
κ^1 Ceti	2012.8, 2013.7	-/-	2001	-/-
ξ Boo A	2013.09	See et al. (2016)	2007.5	Wood and Linsky (2006, 2010)
ab Dor	2001.12, 2002.12	-/-	2001	Testa et al. (2004); Liefke et al. (2008)
ϵ Eri	2007.1, 2008.1, 2010.1, 2011.10, 2012.10, 2013.09	-/-	2001.3	Wood and Linsky (2006)
ξ Boo B	2013.09	See et al. (2016)	2007.5	Wood and Linsky (2006, 2010)
EV Lac	2006.8, 2007.7, 8/	Donati et al. (2008b), See et al. (2016)	2001	Testa et al. (2004); Liefke et al. (2008)
AD Leo	2007.1, 2007.2, 2008.1, 2008.2	-/-	2001	Liefke et al. (2008)
EQ Peg A	2006.8	-/-	2006.11	-/-
EQ Peg B	2006.8	-/-	2006.11	-/-

Table 2:

2.2. Stellar magnetic observations

Inferring parameters of magnetic activity of the fast rotating stars became possible after implementation of Zeeman-Doppler Imaging method (see, Donati and Brown, 1997; Donati, 2001; Donati and Landstreet, 2009). This method is good for determination of the large-scale magnetic field components of stars with a fast rotation rate. This condition makes possible to isolate the rotational dynamics of the Zeeman components in the background spectrum, that is subjected to the Doppler broadening. All stars in our set are rotating faster than the Sun, for example, ϵ Eri and ξ Boo B have the rotational period of ten days and other stars are rotating faster. . They also have the higher magnetic activity. Interesting that the magnetic activity of late-type stars is undoubtedly related with the rotational period (Noyes et al., 1984; Baliunas et al., 1995).

For the fast rotating young suns (having $B-V \sim 0.6$) we used results of Rosén et al. (2016) who used archival observational data of the spectropolarimetric measurements from PolarBase Petit et al. (2014). Results for the K and M-dwarfs are inferred from the data set given by See et al. (2015). All magnetic parameters listed in the Table 1 were calculated using data given in the above cited papers. The proxy parameters P_{AX} and Pr_{Φ} were computed in following the given data sets. Rosén et al. (2016) showed that typical error for the single measurement of the line-of-sight magnetic field can be about 50 percents. However having results for the different rotational phases the error can be reduced substantially. In comparing results of inversions from stellar observations with results from solar magnetic field extrapolation we have to take into account that the WSO pipeline calculates the PFSS (potential field source surface) decomposition assuming that the axisymmetric toroidal magnetic field on the surface is zero, $\overline{B^{(TA)}} = 0$. This may be incorrect (Pipin and Pevtsov, 2014). Also, this is different from procedure employed for studying large-scale magnetic field on the fast rotating stars (see, Donati and Brown, 1997; Donati, 2001; Donati and Landstreet, 2009; Jardine et al., 2017). Note, that Vidotto (2016) considered application of the general procedure, i.e., combination of the PFSS method and a non-zero toroidal magnetic field at the surface, for the SDO magnetic field measurements.

The Table 1 contains results about the coronal chemical composition parameter FIP_{bias} . There we listed parameters given in review of Laming (2015). Recently, Brooks et al. (2017) re-analyzed the data given by Laming (2015) and found that the typical error of the spectrometric inference of the FIP_{bias} is about 10 to 20 percents. The given data show a perfect correlation between spectral class and the FIP_{bias} . Number of stars in our study is smaller because not all the stars shown in Laming (2015) and Brooks et al. (2017) have the magnetic measurements. Also we have to take into account that epochs of observations for the magnetic and chemical composition measurements are very different. The Table 2 shows epochs of observations for each star. Having data from different epochs of observations can bias our conclusion. Therefore analysis of the solar cycle variations of the FIP_{bias} are rather important for understanding the stellar observations.

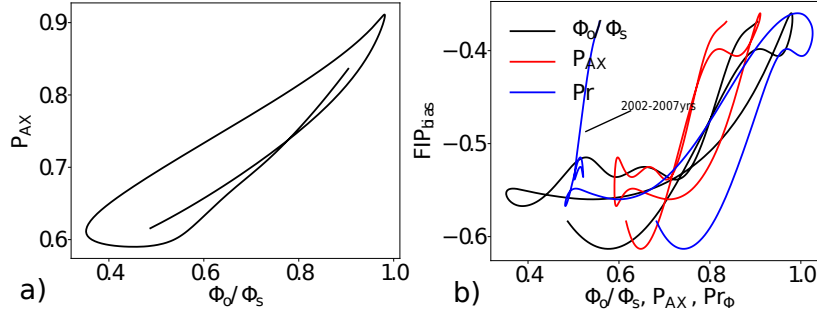


Figure 3: a) Solar cycle correlation between the magnetic fluxes ratio $\Phi_o(t)/\Phi_s(t)$ and the index P_{AX} (see Eq5); b) Solar cycle variations of the FIP_{bias} vs different parameters of solar magnetic activity, such as $\Phi_o(t)/\Phi_s(t)$, P_{AX} and Pr_{Φ} .

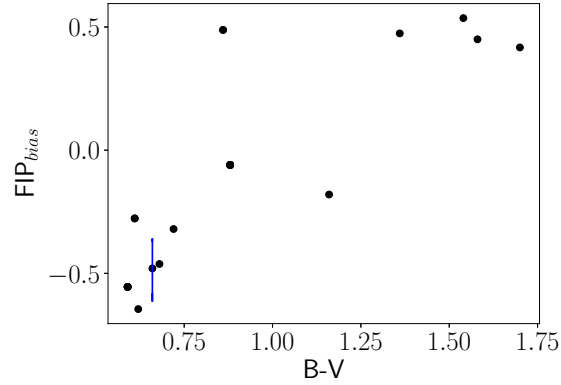


Figure 4: The FIP_{bias} vs the spectral color index B-V (cf, Wood et al., 2012 and Brooks et al., 2017). Blue line shows solar cycle variations of the FIP_{bias} inferred from the Ulysses/SWICS data.

3. Results

Figure 3a shows a close correlation between Φ_o/Φ_s and the introduced index P_{AX} for the smoothed time series. This is not a surprise because the P_{AX} reflect relative strength of the magnetic components which are readily affecting the open and closed magnetic flux of the Sun. Relation between Φ_o/Φ_s and Pr_{Φ} is nonlinear and subjected to the evolutionary trends because of the solar cycle variations. Figure 3b shows that both Φ_o/Φ_s and Pr_{Φ} keep some nonlinear correlation with the coronal chemical composition index FIP_{bias} . Interesting that these correlations had been persisted during the whole period of the Ulysses/SWICS observations. The extended decay of the 24-th solar cycle does not affect much to them. The relation between FIP_{bias} and ratio of the open and closed magnetic flux of the Sun is anticipated from earlier results of Geiss et al. (1995). Here, it is for the first time demonstrated for the Sun as a

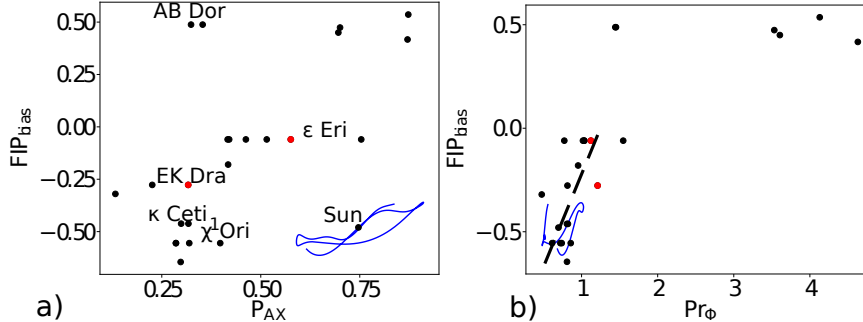


Figure 5: The FIP_{bias} vs the magnetic proxies of the stellar activity. Red circles mark magnetic observations which are close to epochs of measurements of FIP_{bias} (see, the main text).

star that shows a magnetic cycle. We found that the amplitudes of the mean axisymmetric poloidal magnetic field as well as the mean surface toroidal magnetic field could be combined to a good proxy that trace the variations of the total magnetic fluxes and the coronal chemical composition parameter FIP_{bias} . It seems that cycles 23 and 24 have similar magnitude of the FIP_{bias} during epochs of solar maxims. Results of Brooks et al., 2017 shows $FIP_{bias} \approx -0.6$ near in the maximum of the cycle 25. Following to SIDS sunspot data center (<http://sidc.be/silso>) the 25-th solar cycle was considerably lower than cycles 23 and 24. Therefore we can preliminary conclude that the coronal FIP fractionation remains tightly related with the topological properties of the large-scale magnetic field of the Sun, and it is less related with the level of magnetic activity itself. This is partly demonstrated by the index Pr_{ϕ} . Indeed, the relation between Pr_{ϕ} and FIP_{bias} during the first 10 years of the Ulysses observations differs from that during unusually long decay of 24-th solar cycle. This difference is not seen in variation of the FIP_{bias} amplitude. Results of Brooks et al., 2017 confirmed this preliminary conclusion.

Figure 4 reproduces results of Wood et al., 2012 and Brooks et al., 2017 for our sample of stars together with the solar cycle variations of the FIP_{bias} inferred from the Ulysses/SWICS data. Our sample of stars contains less instances than that from Wood et al., 2012 and Brooks et al., 2017. As a result we have a gap for stars with the color index B-V between 1.15 and 1.3 (associating with K6- M2 spectral types). Results of Wood et al., 2012 and Brooks et al., 2017 demonstrated that stars in the gap have a slightly positive FIP_{bias} . Therefore the main sequence late-type stars tend to show a continuous linear variation of the FIP_{bias} with the increase of the color index B-V (decrease of mass). The pre-main solar analog star AB Dor goes out of this relation. Origin of this relation can result from properties of dynamo processes operating inside convective zones of the late-type stars. We will see that analysis the solar-cycle variation of the FIP_{bias} can shed some light on relation of the FIP_{bias} with the stellar color index B-V.

Figure 5 shows the FIP_{bias} vs the calculated magnetic parameters P_{AX} and Pr_{Φ} for our sample of stars. The high dispersion of data is very clear. It is expected because of the very different epochs of measurements of magnetic field and the coronal chemical composition. All the solar like-stars, i.e., those that are partially convective, demonstrate the magnetic activity cycles (Baliunas et al., 1995). Using results of Messina and Guinan (2003); Metcalfe et al. (2013) and Egeland (2017) we put the determined periods in the Table 1. All those stars are younger than the Sun and they show the high variability of the magnetic cycle. Comparing results of Metcalfe et al. (2013) and epoch of observation of the coronal chemical composition for ϵ Eri (young K2-dwarf) we find that the measured FIP_{bias} is related to the epoch of the low activity of the star. The point of the magnetic measurement which is the most close to that phase of the activity of ϵ Eri is marked by the red color. Following to conclusions inferred from solar activity the parameter of the coronal FIP fractionation for the other epochs of the magnetic measurements on ϵ Eri is expected to be higher, i.e., we expect the $FIP_{bias} < -0.06$ in those epochs. The same conclusion can be drawn for EK Dra because of results of Järvinen et al. (2007) and Telleschi et al. (2005). We found that measurements of the FIP_{bias} are related to epoch of the relatively low activity of the EK Dra.

All the young solar analogs in our sample have a strong toroidal magnetic field on the surface. This results to a smaller than for the Sun parameter P_{AX} . As a result, Figure 5a shows the solar cycle variations out of the sample of stars. The amplitude of the horizontal dispersion of stars in Figure 5a is comparable with magnitude of the P_{AX} variations during the solar cycle. The up-right corner of the 5a is occupied by a small sample of M-dwarf stars. Those stars shows the high amplitude of the poloidal magnetic field. This results in the high parameter P_{AX} in that sample. Topology of the large-scale magnetic field of the M-dwarfs resembles the Sun’s magnetic field during the cycle minims. Those stars have poloidal magnetic field of strength 1kG and more (Donati et al., 2008a; Morin et al., 2008). The M-dwarfs show the so-called “reversed” FIP_{bias} (Wood et al., 2012). The “reversed” FIP_{bias} is also found on the AB Dor which represent the pre-main sequence solar analog passing the so-called T-Tauri stage of evolution (Lalitha et al., 2013). Interesting that ratio between the mean magnitudes of the magnetic field components (P_{AX}) on the AB Dor corresponds to that on others young solar analogs in our sample. On the other hand the FIP_{bias} is similar to that found in M-dwarfs and similarly to M-dwarfs, the AB Dor shows rather strong mean density of the poloidal magnetic field.

Figure 5b shows results for the stellar FIP_{bias} against the parameter Pr_{Φ} . The given parameter represents variations of topology of the coronal field and variations of the magnetic activity level, as well. With this parameter dispersion in the solar-types stars sample is much smaller than in Figure 5a. It is seen that the dispersion in the horizontal direction is comparable with that shown by the Sun, and the solar cycle variations of the FIP_{bias} covers the sample of the solar-like stars. We can guess that dispersion is caused by the magnetic cycles on those stars. Also the cloud of sun-like stars is elongated in direction of variations the FIP_{bias} in the solar cycle. We fit the solar analogs sample (including the solar

cycle data) with linear regression:

$$\text{FIP}_{bias} \approx 0.25 - 0.66\text{Pr}_\Phi, \quad (7)$$

where the correlation coefficient between FIP_{bias} and Pr_Φ is 0.67 with zero almost probability for the null hypothesis. The latter is due to deterministic variations of FIP_{bias} vs Pr_Φ the solar cycle (see, Fig3). Excluding the solar cycle data from Figure 5b we get regression: $\text{FIP}_{bias} \approx 0.5 - 0.78\text{Pr}_\Phi$ with correlation coefficient of 0.59 and the null hypothesis probability of 0.02. However the given sample is small and that conclusion is not reliable. The quantitative similarity between results of the small and large samples give some confidence that our result is not an accident. The pre-main sequence star AB Dor is located out of two distinct clouds.

The exceptional properties of AB Dor are rather interesting. On one hand we see that topology of magnetic field of the star is similar to the solar-like stars sample. On other hand the coronal FIP fractionation on AB Dor is probably happened in a way similar to that demonstrated by the M-dwarfs. From our data (Table 1) we also can see that magnitude of the poloidal magnetic field is growing with increasing index B-V (associated with the decreasing stellar mass). This is in agreement with Donati et al. (2008a), Morin et al. (2008) and See et al. (2016). The poloidal magnetic field is an important parameter of the stellar coronal activity. On the solar type stars the large-scale coronal magnetic field is formed from the remnants of the emerging active regions which, in following to Parker's(1955) idea, is supposed to be originated from the large-scale toroidal magnetic fields.

4. Discussion and conclusions

Preliminary results of our analysis can be summarized as follows. The solar cycle variations of the FIP_{bias} show linear relation with balance of the open and close magnetic flux of the Sun as a star. Surprisingly, that the amplitude of variation of ratio Φ_o/Φ_s remained constant during the period of the WSO observations. This agrees with earlier conclusions of Fisk and Schwadron (2001). The ratio Φ_o/Φ_s can be related with parameter P_{AX} that measures a balance between the mean densities of the large-scale poloidal and toroidal magnetic field on the solar surface. Taking into account results of Brooks et al., 2017 we see that the Sun as a star FIP_{bias} keeps running in correlation with parameters Φ_o/Φ_s and P_{AX} , varying in range between -0.6 to -0.4 from cycle 23 to cycle 25. We conclude that the topological characteristic of the large-scale solar coronal magnetic field can be important for the origin of the chemical composition FIP fractionation processes in the coronal plasma. Applying our analysis to the stellar magnetic and spectrometric observations we see the similar tendencies. For example, variations of the stellar FIP_{bias} occurs in the same direction as for the Sun, i.e., increasing amplitude of the poloidal magnetic field results in the increasing of the FIP_{bias} .

One the most interesting theoretical scenario about the origin solar FIP effect was developed by Laming (2015). Comparing to other ideas, e.g., Schwadron

et al. (1999) (also, see review of Tomozov, 2013), the scenario of Laming (2015) has advantage explaining both the normal (solar-like) and the inversed FIP effect from the same mechanism. The key idea behind his model is that the FIP fractionation is induced by the so-called ponderomotive force. This force results from propagation of resonant alfvénic waves along the closed magnetic field lines. Direction and amplitude of the ponderomotive force depends on the gradient of wave energy in the low corona. For the resonant waves the energy grows up and this results in the upward ponderomotive force acting on ions of the low FIP. In the open magnetic field structures and for off-resonant waves the wave energy decreases in the major part of the low corona (see Laming, 2004). Strong reflections of waves from upper boundary of transition region results in inversion of the ponderomotive force and inversion of the FIP effect. The detailed calculations made by Wood et al. (2012) and Laming (2015) demonstrated efficiency of the given mechanism both for the Sun and the M-dwarfs stars.

The given scenario gives a natural explanation for the solar cycle relation between parameters of the open and close magnetic flux and the coronal FIP_{bias} for the Sun as a star. Note that the alfvénic waves is one of the possible mechanism for the solar corona heating (Aschwanden, 2005). Interesting that estimations of Laming (2015) showed that magnitude of the density energy of alfvénic waves is the one that it is necessary for to maintain the magnitude of the FIP_{bias} in magnetic arcade. This density energy of alfvénic waves corresponds to that needed for the coronal heating, as well. From our analysis and results of Brooks et al., 2017 we find that the maximum magnitude of the FIP_{bias} was almost the same during the past three solar maxims. This is contrary to expectation from model of Laming (2015), where the effect depends on the magnitude of the magnetic field. On other hand from Figure 2 we see that the maximum magnitude of the mean density of the toroidal magnetic field did not drop very much. This means that number of the resonant magnetic arcades needed to produce the coronal FIP_{bias} could persists constant. This issue requires further theoretical investigation because the given scenario was never applied to estimate the FIP_{bias} for the Sun as a star. Also, the linear estimations of the ponderomotive force profiles given by Laming (2015) can be inconsistent as we have to take into account the nonlinear effects (see, Shestov et al., 2017).

Laming (2004) and Wood et al. (2012) argued that inversed FIP_{bias} on M-dwarfs can be related with strong reflections of alfvénic waves from upper boundary of transition region. The effect of strong reflections can be caused by a difference of the vertical scales of transition region at the base of the opposite legs of the magnetic arcades (see, Laming, 2004 and Hollweg, 1984). This is expected to find out on active M-dwarfs. Those stars show magnetic field organization which consists of the large-scale patches of strong magnetic field (Donati et al., 2008a). Another possibility for inversion of the FIP_{bias} suggested by Wood et al. (2012) is existence of downward flux of alfvénic waves from corona to chromosphere. The reverse flux of alfvénic waves from corona to chromosphere can be anticipated, as well, because of the strong coronal activity. Roughly speaking the inversion of FIP_{bias} on M-dwarfs can be related with the dramatical increase of magnitude of the coronal magnetic field. The given

mechanisms are considered as a theoretical scenarios which are needed further development.

Final conclusions can be summarized as follows. The solar-like FIP fractionation of the coronal elements is likely related to topology of the large-scale coronal magnetic field. The FIP_{bias} of the Sun as a star varies in solar cycle in reverse proportion to contribution of the open magnetic flux, which depends on ratio the mean density of the large-scale poloidal and toroidal magnetic field on the solar surface. Young solar-like stars tends to demonstrate similar behavior. The restricted amount of data does not allow to conclude about origin of the inversed FIP_{bias} on M-dwarfs stars. Though the available theoretical scenarios suggested that the solar-like FIP_{bias} as well as the inversed FIP_{bias} can be described in the unified picture relating effects of the large-scale topology of magnetic fields and the nonlinear processes of coronal waves propagations.

Acknowledgments We thank support of project II.16.3.1 of ISTP SB RAS. VP thanks the partial support of RFBR grants 15-02-01407 and 16-52-50077.

REFERENCES

References

- Aschwanden, M. J., Dec. 2005. Physics of the Solar Corona. An Introduction with Problems and Solutions (2nd edition).
- Baliunas, S. L., Donahue, R. A., Soon, W. H., Horne, J. H., Frazer, J., Woodard-Eklund, L., Bradford, M., Rao, L. M., Wilson, O. C., Zhang, Q., Bennett, W., Briggs, J., Carroll, S. M., Duncan, D. K., Figueroa, D., Lanning, H. H., Misch, T., Mueller, J., Noyes, R. W., Poppe, D., Porter, A. C., Robinson, C. R., Russell, J., Shelton, J. C., Soyumer, T., Vaughan, A. H., Whitney, J. H., Jan. 1995. Chromospheric variations in main-sequence stars. *ApJ*438, 269–287.
- Brooks, D., Baker, D., van Driel-Gesztelyi, L., Warren, H., 2017. A solar cycle correlation of coronal element abundances in sun-as-a-star observations. *Nature Communications* 8, 183.
URL <https://doi.org/10.1038/s41467-017-00328-7>
- Buergi, A., Geiss, J., Feb. 1986. Helium and minor ions in the corona and solar wind - Dynamics and charge states. *Sol.Phys.*103, 347–383.
- Donati, J.-F., 2001. Imaging the Magnetic Topologies of Cool Active Stars. In: Boffin, H. M. J., Steeghs, D., Cuypers, J. (Eds.), *Astrotomography, Indirect Imaging Methods in Observational Astronomy*. Vol. 573 of *Lecture Notes in Physics*, Berlin Springer Verlag. p. 207.
- Donati, J.-F., Brown, S. F., Oct. 1997. Zeeman-Doppler imaging of active stars. V. Sensitivity of maximum entropy magnetic maps to field orientation. *A & A*326, 1135–1142.

- Donati, J.-F., Jardine, M. M., Petit, P., Morin, J., Bouvier, J., Collier Cameron, A., Delfosse, X., Dintrans, B., Dobler, W., Dougados, C., Ferreira, J., Forveille, T., Gregory, S. G., Harries, T., Hussain, G. A. J., Menard, F., Paletou, F., Apr. 2008a. Magnetic Topologies of Cool Stars. In: van Belle, G. (Ed.), 14th Cambridge Workshop on Cool Stars, Stellar Systems, and the Sun. Vol. 384 of Astronomical Society of the Pacific Conference Series. p. 156.
- Donati, J.-F., Landstreet, J. D., Sep. 2009. Magnetic Fields of Nondegenerate Stars. *An. Rev. Astron. Astroph.*47, 333–370.
- Donati, J.-F., Morin, J., Petit, P., Delfosse, X., Forveille, T., Aurière, M., Cabanac, R., Dintrans, B., Fares, R., Gastine, T., Jardine, M. M., Lignières, F., Paletou, F., Ramirez Velez, J. C., Théado, S., Oct. 2008b. Large-scale magnetic topologies of early M dwarfs. *MNRAS*390, 545–560.
- Duvall, Jr., T. L., Scherrer, P. H., Svalgaard, L., Wilcox, J. M., Mar. 1979. Average photospheric poloidal and toroidal magnetic field components near solar minimum. *Sol.Phys.*61, 233–245.
- Egeland, R., 2017. Long-Term Variability of the Sun in the Context of Solar-Analog Stars. Ph.D. thesis.
- Fisk, L. A., Schwadron, N. A., Oct. 2001. The Behavior of the Open Magnetic Field of the Sun. *ApJ*560, 425–438.
- Fletcher, L., Cargill, P. J., Antiochos, S. K., Gudiksen, B. V., May 2015. Structures in the Outer Solar Atmosphere. *Space Sci. Rev.*188, 211–249.
- Geiss, J., Gloeckler, G., von Steiger, R., Apr. 1995. Origin of the Solar Wind From Composition Data. *Space Sci. Rev.*72, 49–60.
- Hoeksema, J. T., Apr. 1995. The Large-Scale Structure of the Heliospheric Current Sheet During the ULYSSES Epoch. *Space Sci. Rev.*72, 137–148.
- Hollweg, J. V., Feb. 1984. Resonances of coronal loops. *ApJ*277, 392–403.
- Jardine, M., Vidotto, A. A., See, V., Feb. 2017. Estimating stellar wind parameters from low-resolution magnetograms. *MNRAS*465, L25–L29.
- Järvinen, S. P., Berdyugina, S. V., Korhonen, H., Ilyin, I., Tuominen, I., Sep. 2007. EK Draconis. Magnetic activity in the photosphere and chromosphere. *A & A*472, 887–895.
- Lalitha, S., Fuhrmeister, B., Wolter, U., Schmitt, J. H. M. M., Engels, D., Wieringa, M. H., Dec. 2013. A multi-wavelength view of AB Doradus outer atmosphere . Simultaneous X-ray and optical spectroscopy at high cadence. *A & A*560, A69.
- Laming, J. M., Oct. 2004. A Unified Picture of the First Ionization Potential and Inverse First Ionization Potential Effects. *ApJ*614, 1063–1072.

- Laming, J. M., Dec. 2015. The FIP and Inverse FIP Effects in Solar and Stellar Coronae. *Living Reviews in Solar Physics* 12, 2.
- Liefke, C., Ness, J.-U., Schmitt, J. H. M. M., Maggio, A., Dec. 2008. Coronal properties of the EQ Pegasi binary system. *A & A* 491, 859–872.
- Marsden, S. C., Petit, P., Jeffers, S. V., Morin, J., Fares, R., Reiners, A., do Nascimento, J.-D., Aurière, M., Bouvier, J., Carter, B. D., Catala, C., Dintrans, B., Donati, J.-F., Gastine, T., Jardine, M., Konstantinova-Antova, R., Lanoux, J., Lignières, F., Morgenthaler, A., Ramirez-Vélez, J. C., Théado, S., Van Grootel, V., BCool Collaboration, Nov. 2014. A BCool magnetic snapshot survey of solar-type stars. *MNRAS* 444, 3517–3536.
- Messina, S., Guinan, E. F., Oct. 2003. Magnetic activity of six young solar analogues II. Surface Differential Rotation from long-term photometry. *A & A* 409, 1017–1030.
- Metcalfe, T. S., Buccino, A. P., Brown, B. P., Mathur, S., Soderblom, D. R., Henry, T. J., Mauas, P. J. D., Petrucci, R., Hall, J. C., Basu, S., Feb. 2013. Magnetic Activity Cycles in the Exoplanet Host Star epsilon Eridani. *ApJL* 763, L26.
- Morin, J., Donati, J.-F., Petit, P., Delfosse, X., Forveille, T., Albert, L., Aurière, M., Cabanac, R., Dintrans, B., Fares, R., Gastine, T., Jardine, M. M., Lignières, F., Paletou, F., Ramirez Velez, J. C., Théado, S., Oct. 2008. Large-scale magnetic topologies of mid M dwarfs. *MNRAS* 390, 567–581.
- Noyes, R. W., Weiss, N. O., Vaughan, A. H., Dec. 1984. The relation between stellar rotation rate and activity cycle periods. *ApJ* 287, 769–773.
- Parker, E., 1955. Hydromagnetic dynamo models. *Astrophys. J.* 122, 293–314.
- Petit, P., Louge, T., Théado, S., Paletou, F., Manset, N., Morin, J., Marsden, S. C., Jeffers, S. V., May 2014. PolarBase: A Database of High-Resolution Spectropolarimetric Stellar Observations. *Publications of the Astron. Soc. of Pacific* 126, 469.
- Pipin, V. V., Pevtsov, A. A., Jul. 2014. Magnetic Helicity of the Global Field in Solar Cycles 23 and 24. *ApJ* 789, 21.
- Pottasch, S. R., 1963. The lower solar corona: the abundance of iron. *MNRAS* 125, 543.
- Reiners, A., Dec. 2012. Observations of Cool-Star Magnetic Fields. *Living Reviews in Solar Physics* 9, 1.
- Rosén, L., Kochukhov, O., Hackman, T., Lehtinen, J., Sep. 2016. Magnetic fields of young solar twins. *A & A* 593, A35.
- Schatten, K. H., Wilcox, J. M., Ness, N. F., Mar. 1969. A model of interplanetary and coronal magnetic fields. *Sol.Phys.* 6, 442–455.

- Schrijver, C. J., Harvey, K. L., Mar. 1994. The photospheric magnetic flux budget. *Sol.Phys.*150, 1–18.
- Schwadron, N. A., Fisk, L. A., Zurbuchen, T. H., Aug. 1999. Elemental Fractionation in the Slow Solar Wind. *ApJ*521, 859–867.
- See, V., Jardine, M., Vidotto, A. A., Donati, J.-F., Boro Saikia, S., Bouvier, J., Fares, R., Folsom, C. P., Gregory, S. G., Hussain, G., Jeffers, S. V., Marsden, S. C., Morin, J., Moutou, C., do Nascimento, J. D., Petit, P., Waite, I. A., Nov. 2016. The connection between stellar activity cycles and magnetic field topology. *MNRAS*462, 4442–4450.
- See, V., Jardine, M., Vidotto, A. A., Donati, J.-F., Folsom, C. P., Boro Saikia, S., Bouvier, J., Fares, R., Gregory, S. G., Hussain, G., Jeffers, S. V., Marsden, S. C., Morin, J., Moutou, C., do Nascimento, J. D., Petit, P., Rosén, L., Waite, I. A., Nov. 2015. The energy budget of stellar magnetic fields. *MNRAS*453, 4301–4310.
- Shestov, S. V., Nakariakov, V. M., Ulyanov, A. S., Reva, A. A., Kuzin, S. V., May 2017. Nonlinear Evolution of Short-wavelength Torsional Alfvén Waves. *ApJ*840, 64.
- Skumanich, A., Feb. 1972. Time Scales for CA II Emission Decay, Rotational Braking, and Lithium Depletion. *ApJ*171, 565.
- Telleschi, A., Güdel, M., Briggs, K., Audard, M., Ness, J.-U., Skinner, S. L., Mar. 2005. Coronal Evolution of the Sun in Time: High-Resolution X-Ray Spectroscopy of Solar Analogs with Different Ages. *ApJ*622, 653–679.
- Testa, P., Drake, J. J., Peres, G., Dec. 2004. The Density of Coronal Plasma in Active Stellar Coronae. *ApJ*617, 508–530.
- Tomozov, V., 2013. On regularities of distribution of chemical composition in atmospheres of stars. *Solnecho-zemnaya fizika* 23, 23–32.
- Vidotto, A. A., Jun. 2016. The magnetic field vector of the Sun-as-a-star. *MNRAS*459, 1533–1542.
- Vidotto, A. A., Gregory, S. G., Jardine, M., Donati, J. F., Petit, P., Morin, J., Folsom, C. P., Bouvier, J., Cameron, A. C., Hussain, G., Marsden, S., Waite, I. A., Fares, R., Jeffers, S., do Nascimento, J. D., Jul. 2014. Stellar magnetism: empirical trends with age and rotation. *MNRAS*441, 2361–2374.
- von Steiger, R., Geiss, J., Gloeckler, G., Galvin, A. B., Apr. 1995. Kinetic Properties of Heavy Ions in the Solar Wind From SWICS/Ulysses. *Space Sci. Rev.*72, 71–76.
- Widing, K. G., Feldman, U., Jul. 2001. On the Rate of Abundance Modifications versus Time in Active Region Plasmas. *ApJ*555, 426–434.

- Wood, B. E., Laming, J. M., Karovska, M., Jul. 2012. The Coronal Abundance Anomalies of M Dwarfs. *ApJ*753, 76.
- Wood, B. E., Linsky, J. L., May 2006. Coronal Emission Measures and Abundances for Moderately Active K Dwarfs Observed by Chandra. *ApJ*643, 444–459.
- Wood, B. E., Linsky, J. L., Jul. 2010. Resolving the ξ Boo Binary with Chandra, and Revealing the Spectral Type Dependence of the Coronal "FIP Effect". *ApJ*717, 1279–1290.